Crack Path Selection at the Interface of Wrought and Wire + Arc Additive Manufactured Ti-6Al-4V

Jikui Zhang[a], Xiang Zhang[*,b,c], Xueyuan Wang[b,c], Jialuo Ding[b], Yéli Traoré[d]
Sanjooram Paddea[d], Stewart Williams[b]

[a] Department of Aircraft Design, Beihang University, Beijing, 100191, P.R. China
[b] School of Aerospace, Transport and Manufacturing, Cranfield University, Bedford MK43 0HQ, UK
[c] Faculty of Engineering, Environment and Computing, Coventry University, Coventry CV1 2JH, UK
[d] The Open University, Walton Hall, Milton Keynes MK7 6AA, UK

Abstract

Crack propagation deviation tendency in specimens containing an interface between wrought alloy substrate and Wire + Arc Additive Manufacture (WAAM) built Ti-6Al-4V is investigated from the viewpoints of microstructure, residual stress and bi-material system. It is found that a crack initiated at the interface tends to grow into the substrate that has equiaxed microstructure and lower resistance to fatigue crack propagation. Experimental observations are interpreted by finite element modelling of the effects of residual stress and mechanical property mismatch between the WAAM and wrought alloy. Residual stresses retained in the compact tension specimens are evaluated based on measured residual stress in the initial WAAM built wall. Cracks perpendicular to the interface kept a straight path owing to the symmetrical residual stress distribution. In this case the tangential stress in bi-material model is also symmetric and has the maximum value at the initial crack plane. In contrast, cracks parallel to the interface is inclined to grow towards the substrate due to the mode II (or sliding mode) stress intensity factor caused by the asymmetric residual stress field. Asymmetric tangential stress in the bi-material model also contributes to the observed crack deviation trend according to the maximum tangential stress criterion.

Keywords: additive manufacturing, titanium alloy, crack path selection, microstructure, residual stress, bi-material, finite element model

1. Introduction

Due to their excellent mechanical properties and corrosion resistance, high strength titanium alloys are extensively used as a key structural material in the aerospace industry. At present, titanium parts are mostly fabricated by the conventional wrought based processes such as machining from solid billets and therefore have a very high buy-to-fly ratio [1]. The new additive manufacturing (AM) technology has proved a highly effective method to reduce the production time and cost comparing with the traditional manufacturing process. The Wire + Arc Additive Manufacture (WAAM) process [2,3], which feeds a wire at a controlled rate into an electric or plasma arc to melt the wire onto a substrate or the previously deposited layer, is a developing AM technology that has found applications in the aerospace and other industrial sectors. Compared to the powder-based AM processes, WAAM has a much higher material deposition rate, lower process cost and no powder handling requirement [4]. However a higher amount of post process machining is required due to the lower dimensional accuracy and surface roughness. WAAM is very promising for fabricating large components in high strength titanium alloys.

---

[*] Corresponding author at: Coventry University, Faculty of Engineering, Environment and Computing

E-mail addresses: zjk@buaa.edu.cn (J. Zhang); xiang.zhang@coventry.ac.uk (X. Zhang); jialuo.ding@cranfield.ac.uk (J. Ding); sanjooram.paddea@open.ac.uk (S. Paddea); s.williams@cranfield.ac.uk (S.Williams)

One of the main challenges to the widespread use of AM technologies to produce safety critical structural components has been widely recognised as the issues of material properties and repeatability [5, 6]. So far a number of studies have been conducted in this area for AM Ti-6Al-4V (referred to as Ti-6-4 in the text). These include the static strength, ductility, high cycle fatigue and fracture toughness properties of wire based AM [6-10], powder bed selective laser melting (SLM) [11-14] and powder bed electron beam melting (EBM) [15]. Fatigue crack growth behavior has also been studied in SLM and EBM Ti-6-4 [11, 14, 15]. However, there is no published work yet on fatigue crack growth rates in the wire based AM metals. Furthermore, AM metal may be required to be built on to a substrate in practice; hence the need to study crack growth behaviour at the interface of two different alloys in order to apply the AM alloys in realistic structural assemblies or repairs. Since the damage tolerance design requirement requires not only the fatigue crack growth properties but also modelling and predictive tools, it is very important to study the influence of microstructure and residual stress that are identified as the key factors for WAAM built Ti-6-4 [16].

The conventional $\alpha+\beta$ forging processes are widely used to for the high strength Ti-alloy to obtain a typical equiaxed or bi-modal microstructure with excellent mechanical properties [17]. Many studies have been conducted to investigate the microstructure and mechanical properties of AM deposited titanium alloys. Previous studies [3, 4] have shown that the β grain of WAAM Ti-6-4 is similar to those in powder bed AM alloys deposited by SLM [18] or EBM [19, 20]. The microstructure of WAAM Ti-6-4 consists of fine Widmanstätten α in the upper deposited layers and a banded coarsened Widmanstätten lamella α in the lower layers [9], which is quite different from the equiaxed or bi-modal microstructure of the high strength Ti-6-4 in wrought condition. The coarse lamellar microstructure is also observed for other AM process produced titanium alloys [8, 9, 20] and is found to retard the crack growth rate [17, 21]. The difference in the microstructure results in different mechanical properties. WAAM Ti-6-4 has slightly lower yield and ultimate tensile strengths than those of forged bar, the ductility is comparable but the high cycle fatigue life is significantly higher [9, 22]. Furthermore, the as-deposited WAAM Ti-6-4 exhibits direction dependent mechanical properties. In the literature, the welding torch movement direction is defined as the longitudinal direction (L) and the layer building direction is the transverse (T), see Fig.1. The average yield and ultimate tensile strengths are higher in the longitudinal direction than that in the transverse direction [7]. Fatigue crack growth rate is also slightly greater in the longitudinal than the transverse direction [23]. For the SLM [14] and EBM Ti-6-4 [15], no noticeable difference was observed in the crack growth rate in the Paris law region between the two directions.
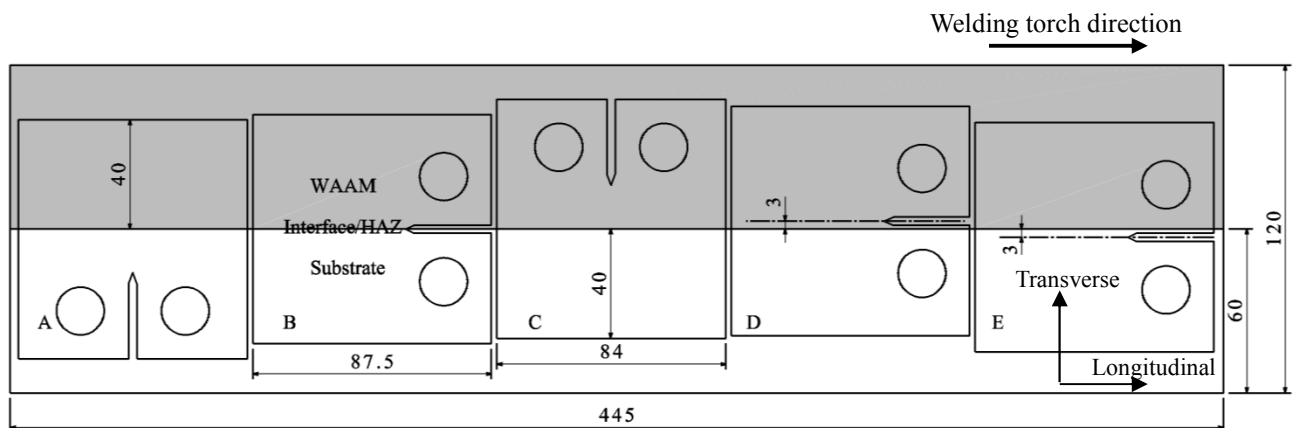

Fig. 1 Layout of test specimens on a WAAM-substrate wall showing the WAAM-substrate interface location on each type of C(T) specimen (unit: mm)

Differences in the microstructure and mechanical properties in the wrought and WAAM conditions raise another issue for the designers. WAAM deposited on to a wrought substrate makes a bi-material system with an interface region. Crack path selection and the interface fracture property in bi-material systems has previously been studied [24]. The crack trajectory in a bi-material system depends on the local properties and local stress and strain field. For example, in a laser beam welded aluminum alloy sheet, it is observed that crack extends towards the softer fusion zone that has much lower yield strength than the base metal [25]. The bi-material interface regions are found to be the weakest location for material failure due to the microstructure and mechanical property heterogeneity [26]. Therefore, understanding the crack growth behavior at the bi-material interface is very important to improve the structural integrity design of WAAM deposited components.

Residual stress caused by the thermal contraction of the melting materials [27] is another key factor that can impact the crack growth behavior. Residual stress can be either beneficial or detrimental depending on its sign, magnitude, distribution and interaction with the service load induced stress field. Attempts have been made to quantify residual stress in AM parts [27-29]. For example, the neutron diffraction method was used to probe parts produced by the LENS method (a powder based AM process) and found significant compressive residual stress within a built component [28], which were observed to increase the fatigue life as the compressive stress caused crack tip closure; hence retarding the crack growth rate. Another study [29] showed that the peak residual stress shifted as weld beads were added to previous welds and can have the beneficial effect of lowering the peak stress, particularly in the weld toe area, which is a common site of in-service cracking. It should be pointed out that cracking occurs perpendicular to the deposited layers in [28, 29]. The influence of residual stress on cracks running parallel to the deposited layers is not found in the open literature.

Experimental tests have been conducted to study the fatigue crack growth behaviour of WAAM deposited Ti-6-4 by our research group [30-32]. A recent paper [33] reported the effects of microstructure and residual stress on the growth behavior of crack perpendicular to the WAAM-substrate interface. This paper aims to understand the path selection of a crack at the interface either perpendicular or parallel to the interface. Firstly, fatigue crack growth test of compact tension specimens from previous tests is introduced. Subsequently, finite element models are presented for calculating residual stresses retained in the test specimens and resultant stress intensity factors, and investigating the crack path selection in the bi-material system (substrate and WAAM alloys). Finally, crack path selection issues are discussed from the viewpoints of microstructure, residual stress and bi-material system, respectively.

2. Experimental

2.1 Manufacturing process and experimental setup

Fatigue tests of compact tension, C(T), specimens were conducted at Cranfield University [30-32] to investigate crack growth behavior at the WAAM-substrate interface. The specimens were machined from a "wall" (Fig. 1) fabricated by the Welding Engineering and Laser Processing Centre at Cranfield University using the WAAM technology using process parameters given in Table 1 [30]. A total of four walls were manufactured for this project. One of them was used for residual stress measurement; the other three were used to produce the test specimens shown in Fig. 1. Five C(T) specimens were machined from each wall to fatigue test standard. Fig. 2 shows the geometry and the dimension of the C(T) specimens complying with the ASTM standard [34]. The nominal thickness is 6 mm.

Five different crack scenarios (Fig. 1) were investigated on the fatigue crack growth pattern at the WAAM-substrate interface, which are potentially important for design considerations. Fatigue tests

were conducted using an Instron Model 8031 servo-hydraulic test machine in the following two steps: (1) pre-crack of 3 mm was prepared to eliminate the effect of the machined notch root. At the load ratio 0.1, the maximum load was kept at 6 kN for pre-cracking to 2.5 mm length and then reduced to 5 kN for a further 0.5 mm crack growth. (2) Crack growth tests were conducted under the maximum load of 5 kN and load ratio 0.1. A travelling microscope of ×7 magnification factor was used to monitor the crack tip location. The loading frequency was 10 Hz for both the pre-cracking and fatigue crack growth tests. Three specimens were tested for each geometry type.

Table 1 Build parameters used for the production of the WAAM-Substrate wall [30]

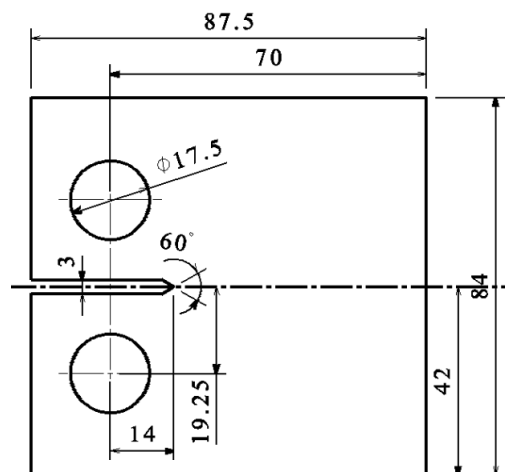| Layers	1-3	4-6	7-9	>9
Current(A)	160	155	150	145
Arc voltage(V)		20.4		
Wire feed speed (mm/s)		33.33		
Travel speed (mm/s)		4.5		
Plasma gas flow rate (l/min)		0.8		
Torch shielding gas rate (l/min)		8		
Wire diameter (mm)		1.20		
Layer height (mm)		1.25		

Fig. 2 Geometry and dimension of WAAM build C(T) specimen (unit: mm)

2.2 Fatigue crack trajectory

Figure 3 presents the crack growth trajectory observed on polished specimen surfaces. The photos are presented in two categories by the applied load direction versus the WAAM-substrate interface.

(1) Applied load parallel to the WAAM-substrate interface: specimen Type A (crack initiates from the substrate and propagates into the WAAM alloy) and Type C (crack initiates from the WAAM alloy and propagates into the substrate). The crack was found to maintain a straight line perpendicular to the interface for both specimens as shown in Figs. 3a and 3c. This is attributed to both the geometry and load symmetry. As shown in the previous work [33], residual stresses and microstructure only affected the crack growth rate, but not the crack propagation trajectory.

(2) Applied load perpendicular to WAAM-substrate interface: Type B (initial crack at the interface), Type D (initial crack in the WAAM alloy, 3 mm above the interface) and Type E (initial crack about 3 mm below the interface, in the heat affected zone (HAZ) on the substrate side). Figs. 3b, d and e show that the cracks in these specimens all propagated into the substrate even if it is 3 mm away from the

interface. Although the applied load is symmetric, the microstructure and material properties are different on either side of the crack, which may have affected the crack path selection. Process induced residual stress is another factor that can influence the crack path selection by altering the crack tip stress distribution.
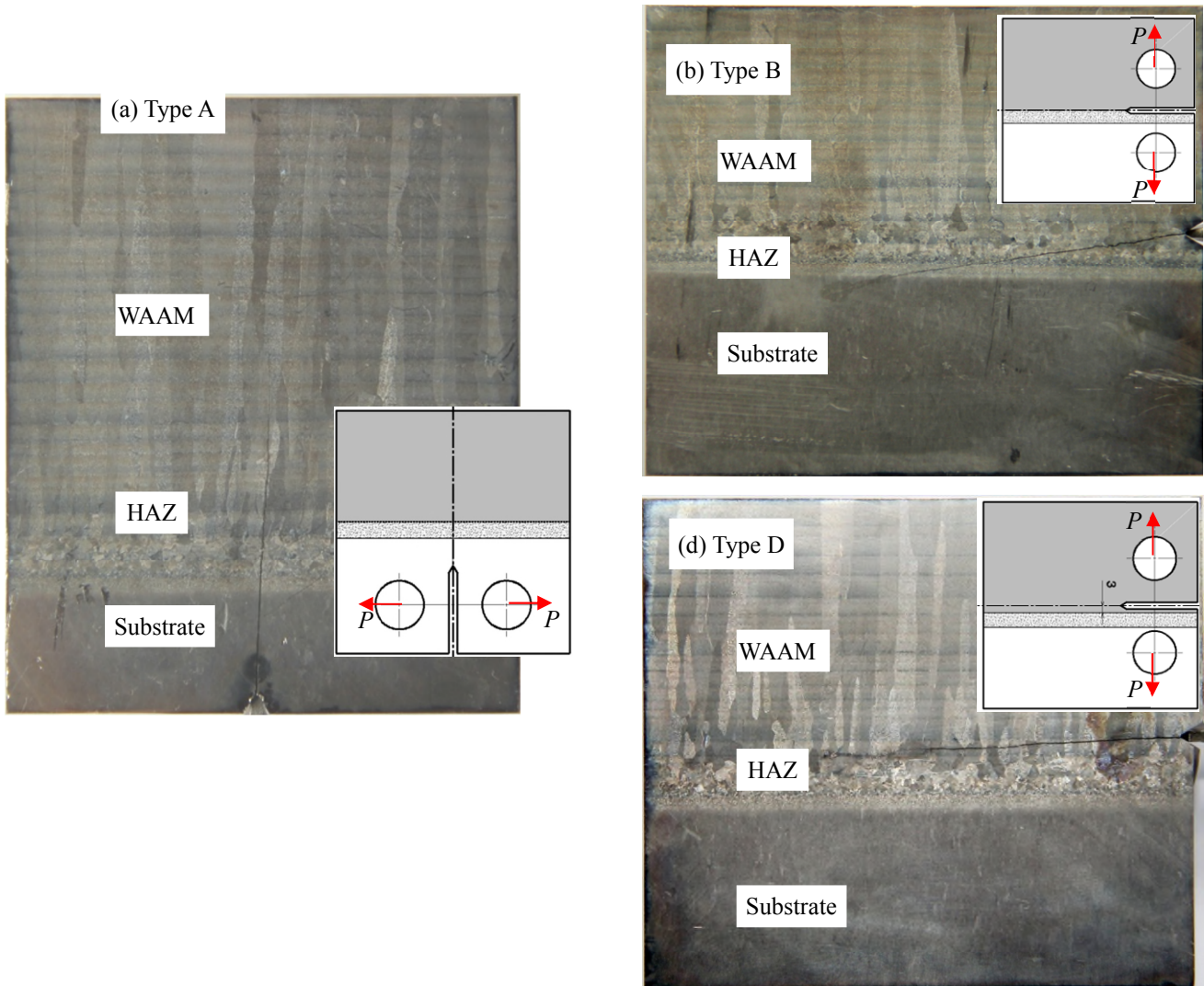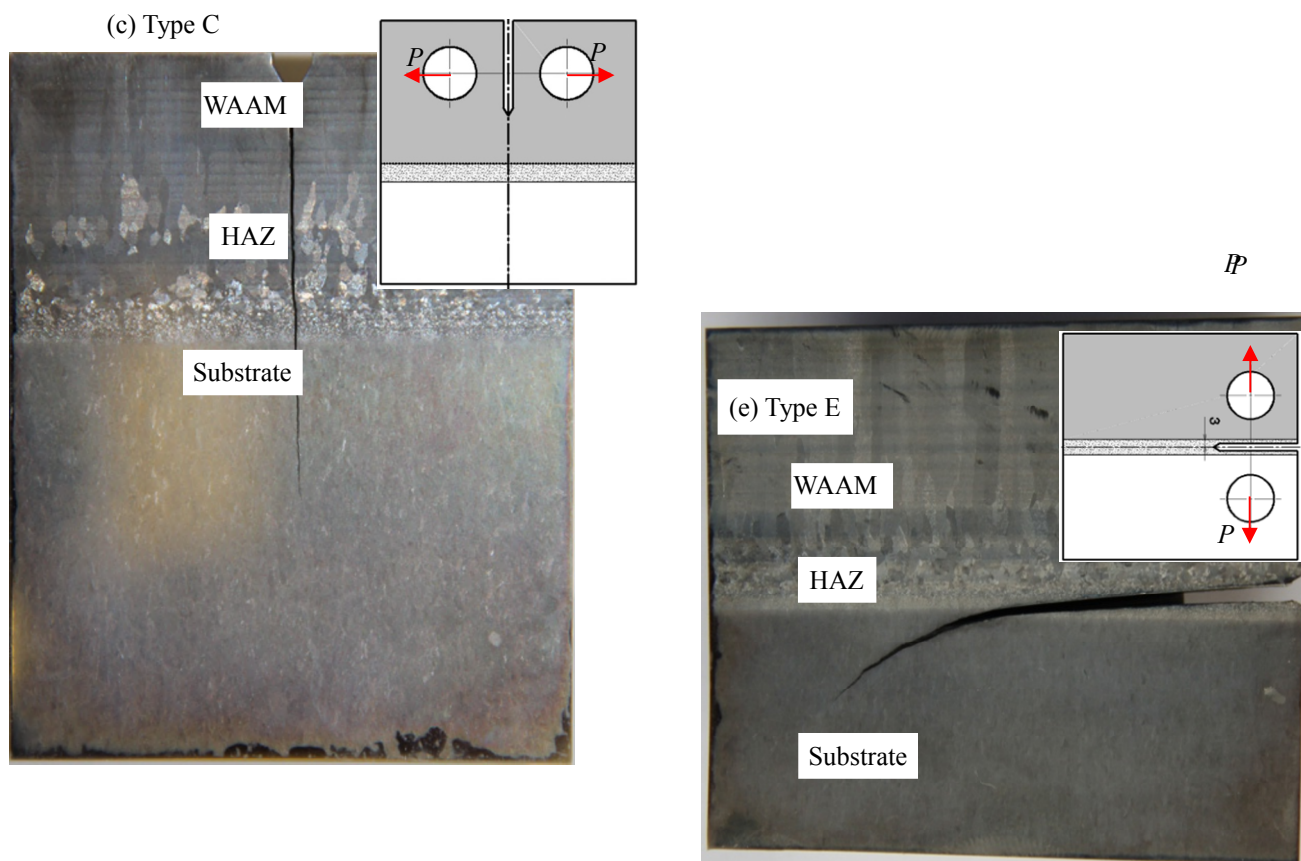
Fig. 3 Macroscopic photographs showing fatigue crack trajectory in the interface of WAAM-substrate C(T) specimens.

2.3 Measurement of the residual stress

To validate the residual stress prediction model presented in [33], residual stresses retained in Type B specimen were measured by the contour method [35]. The contour method involves cutting the component of interest into two parts, measuring the relaxed deformation profile of the cut surfaces and applying this profile as boundary conditions in an elastic finite element (FE) analysis to back-calculate the original out-of-plane residual stress field at the cut face.

The cutting process was conducted using an Agie Charmilles wire EDM machine (FI-440CS) with a 100 μm brass wire diameter. The specimen was 'finger' clamped on the wire EDM bed to avoid any free movement during the cutting operation. Once the cutting process was completed, the distorted cut faces were measured using a Zeiss Eclipse co-ordinate measuring machine (CMM), fitted with a Micro-Epsilon laser probe and a 4 mm diameter ruby-tipped Renishaw PH10M touch trigger probe. The measurement spacing adopted was on a 0.1 mm square grid.

Noise in the measured surface contour is unavoidable due to the nature of the EDM cut surfaces and uncertainty in CMM measurements. Because the stress calculation magnifies the noise in the data, it is important to smooth the surface deformation data. In the present work data smoothing was conducted using cubic spline fitting. For this purpose, several 'knot spacings' (1x1, 2x2, 3x3, 5x5 and 7x7 mm^2) were examined. The uncertainty in the calculated stresses at any given node on the cut surface was estimated by taking the standard deviation of the new stress and the stress from the previous, coarser

fit [36]. The minimum average stress uncertainty was 6.4 MPa which corresponded to an optimum knot spacing of 3x3 mm^2 in this case.

A 3D linear elastic FE analysis was performed using the ABAQUS code to calculate the residual stress from the applied deformation at the cut surface. The 3D FE model of the specimen was generated using the perimeter of the cut face measured by the CMM. The elastic properties (Young's modulus and Poisson's ratio) of the test specimen were defined and residual stresses back-calculated by applying the opposite of the smoothed deformation contour to the cut plane as boundary conditions. Measured stress profile is compared with FE prediction and presented in Section 3.1.

3. Finite element analysis

3.1 Residual stress effect on crack path selection
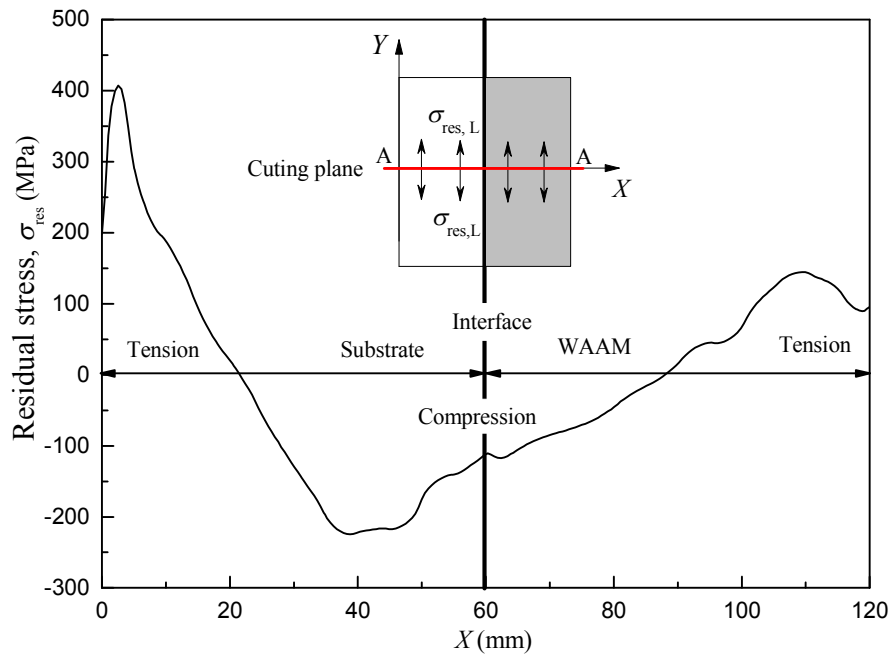
3.1.1. Residual stress in C(T) specimens

An elastic FE model was developed to simulate cutting of C(T) specimen from the WAAM wall in our previous paper [33]. The specimen cutting process can be regarded as a stress relief process due to material removal [37]. An element removal model is available in ABAQUS [38] that can be used to remove parts from an initially built model to simulate the machining process.

Residual stresses retained in the Type A and C specimens, i.e. crack perpendicular to the interface, are reported in [33]. Before removing any material, the measured residual stress field in the wall (Fig. 4) is put into the FE model as the initial stress condition using a user defined subroutine (designated as SIGINI in ABAQUS). To model the residual stress in type B specimen (crack parallel to the interface), C(T) specimen model and refined mesh with singularity elements around the crack tip are illustrated in Fig. 5. The modelling procedure is the same as in [33]. To validate the FE model, Fig. 6 compares the FE calculated and test measured residual stresses retained in the B specimen prior to the fatigue crack propagation test. Prediction is in good agreement with the test.
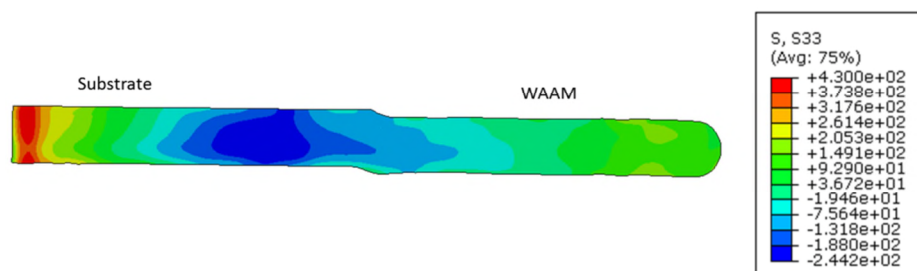
(a) 2D normal stress map in the cutting plane A-A

(b) 1D normal stress profile along the line of mid-thickness

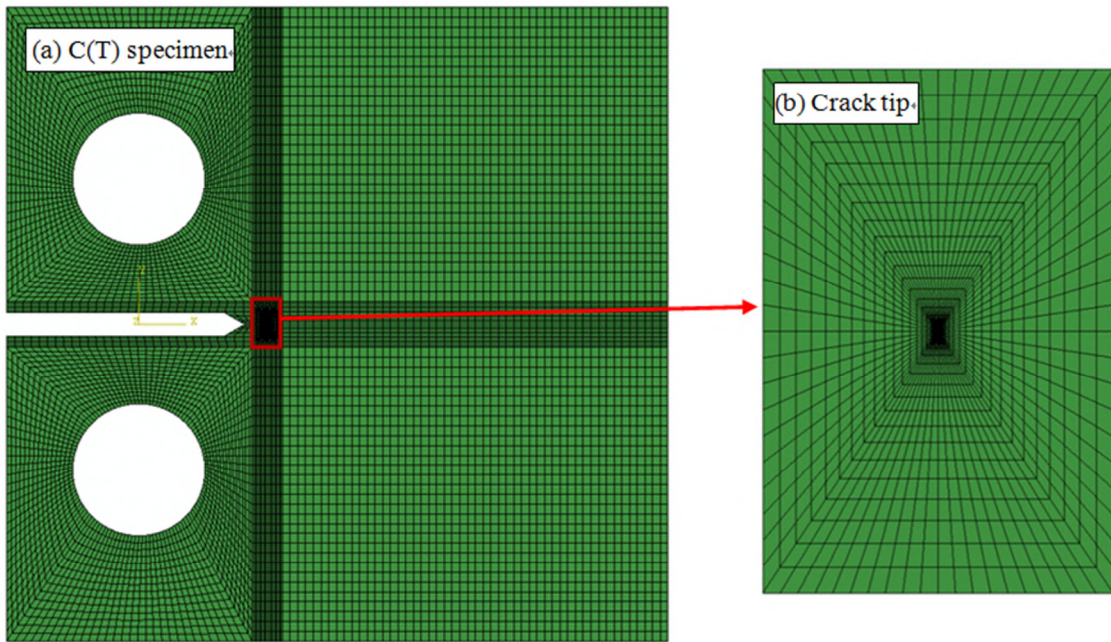Fig. 4 Measured residual stress in the wall

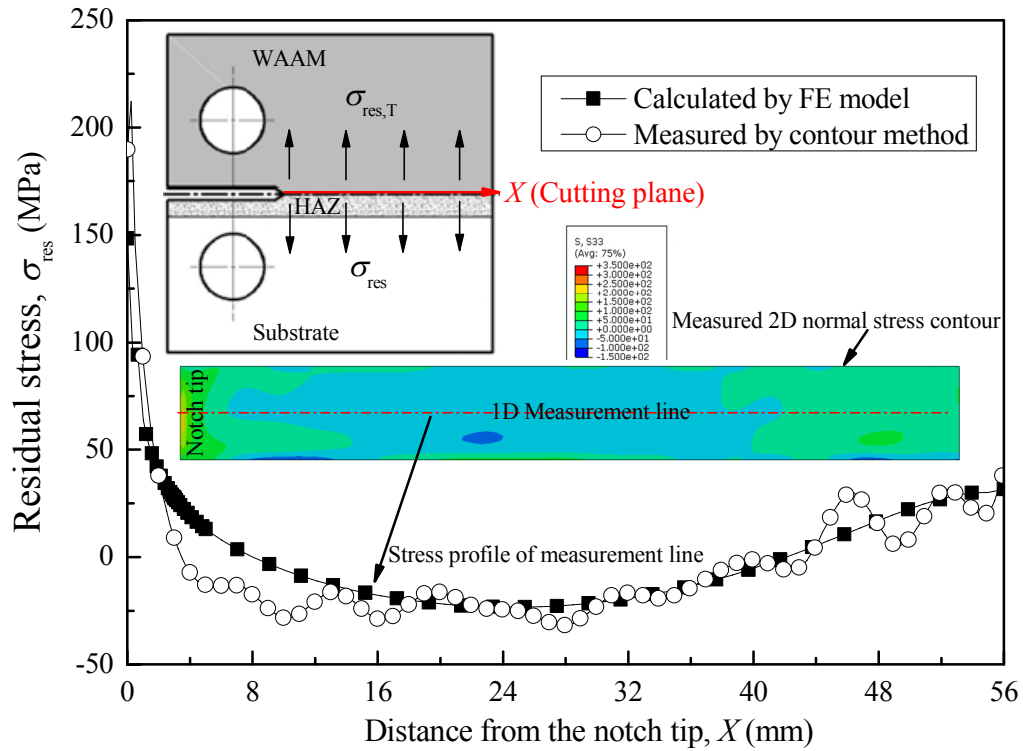Fig. 5 Finite element model for calculating residual stress retained in C(T) specimen

Fig. 6 Residual normal stress retained in the Type B specimen (with notch, no crack)

Bearing in mind that the aim of this paper is to understand the crack path selection near the WAAM-substrate interface, a longer crack length was used in the FE model, i.e. 30 mm for Type A and C so that the crack tip is located at the interface. For the Type B, D and E specimens, a 17 mm crack length was used in the FE models (representing 14 mm notch plus 3 mm pre-crack). Calculated residual stress distributions near the crack tip are shown in Figs. 7 and 8. Calculated residual stress intensity factors (K_{res}) are extracted from the contour (J)-integral and given in Table 2. From these results, following observations can be drawn:

(1) For the Type A and C specimens, the residual stress distribution (Fig. 7) is symmetric when the crack initiates and propagates perpendicular to the WAAM-Substrate interface. The resultant mode I stress intensity factors ($K_{I,res}$) are 1.50 MPa$\sqrt{m}$ for Type A specimen and 10.183 MPa$\sqrt{m}$ for Type C when a = 30 mm (crack tip at the WAAM-substrate interface). The mode II residual stress intensity factor ($K_{II,res}$) is zero for both specimens as shown in Table 2, indicating that the influence of residual stress is limited to increasing the total mode I stress intensity factor and subsequently increasing the crack growth rate, but not changing the crack trajectory (pure mode I crack propagation). This explains the straight crack path on the Type A and C specimens (Figs. 3a and c).

(2) For the Type B, D and E specimens, residual stress distribution and induced deformation (Fig. 8) are apparently asymmetric. Calculated values of residual stress induced stress intensity factor (K_{res}) in Table 2 indicate that K_{res} is considerable for both the mode I and mode II crack growth. Consequently the crack propagated under the mixed mode, i.e., the crack path deviated from the expected path (Fig. 3b, d, e) due to the asymmetric residual stress distribution. The deviation angle depends on the proportion of the applied load to the residual stress magnitude.
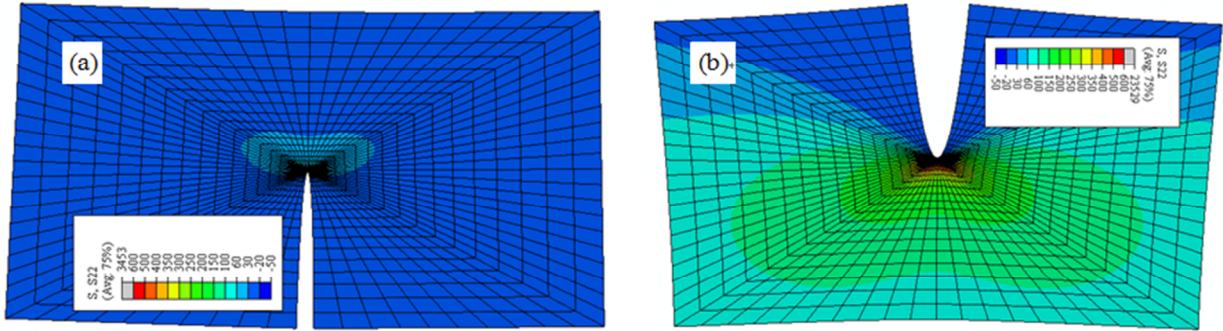
Fig. 7 Residual stress (σ_{22}) in the crack tip of C(T) specimens, (a) Type A, (b) Type C
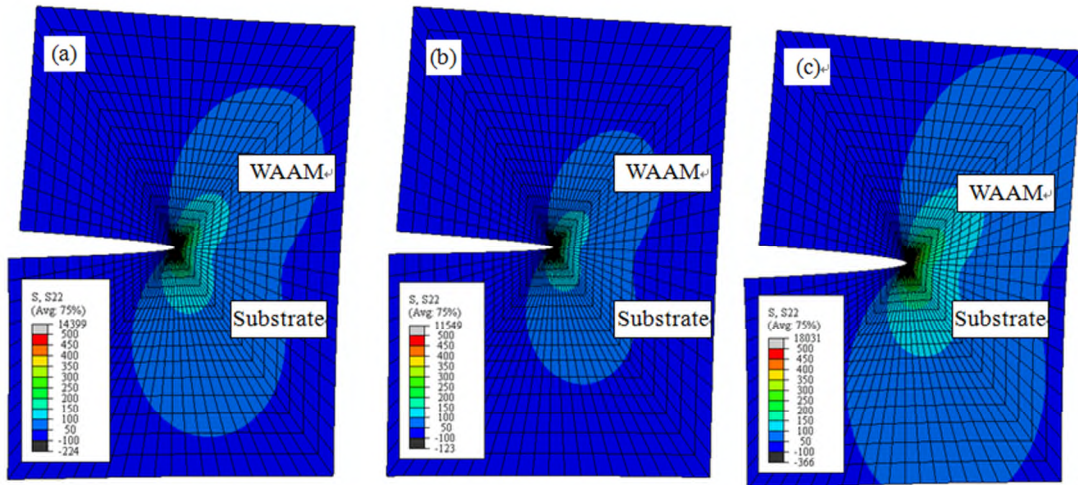(Refined singularity mesh region around the crack tip: 6 mm × 4 mm)

Fig. 8 Residual stress (σ_{22}) in the in the crack tip of C(T) specimens, (a) Type B, (b) Type D (c) Type E
(Refined singularity mesh region around the crack tip: 6 mm × 4 mm)

Table 2 Residual stress induced stress intensity factor (K_{res}) for the C(T) specimen

Type of Specimen	A	B	C	D	E
Crack length, a (mm)	30	17	30	17	17
K_{res} of mode Ⅰ, $K_{I,res}$ (MPa$\sqrt{m}$)	1.502	5.850	10.183	4.743	7.242
K_{res} of mode Ⅱ, $K_{II,res}$ (MPa$\sqrt{m}$)	0.000	2.704	0.000	1.771	3.731

3.1.2. Maximum tangential stress criterion (elastic stress field)

The influence of residual stress distribution on crack deviation angle is determined by the maximum tangential stress criterion (elastic) that is available in ABAQUS [39]

$$\theta = \cos^{-1} \frac{3K_{II}^2 + \sqrt{K_I^4 + 8K_I^2 K_{II}^2}}{K_I^2 + 9K_{II}^2} \tag{1}$$

where, crack deviation angle (θ) is measured counterclockwise with respect to the initial crack plane, i.e. $\theta = 0$ represents crack propagation in the "straight-ahead" direction when $K_{II}=0$, whereas $\theta < 0$ if $K_{II}>0$ or $\theta > 0$ if $K_{II}<0$. Values of K_I and K_{II} depend on the proportion of applied maximum load to the residual stress magnitude that is calculated by FE model in Section 3.1.1. Calculated crack deviation angles are presented in Section 4.3.

3.2 Crack path selection in the bi-material system

Mechanical properties of WAAM and wrought Ti-6-4 are given in Table 3. The WAAM alloy has a higher Young's modulus but lower yield and ultimate tensile strength in both the longitudinal and transverse directions. When a crack is adjacent to the WAAM-substrate interface, it could be regarded as propagating in a bi-material system having different mechanical properties between the two process conditions. Consequently, a complex stress field is found around the crack tip owing to the elastic and plastic mismatch [40]. An elastic-plastic FE model is developed in this paper to predict the crack path selection due to the elastic (Young's modulus) and plastic (yield strength) mismatch.

Table 3 Mechanical properties of WAAM and substrate Ti-6Al-4V [7, 23]

Material	Direction	Young's modulus (GPa)	Yield strength (MPa)	Ultimate tension strength (MPa)
WAAM	Longitudinal	123.5	840	923
	Transversal	126.5	810	906
Substrate	Isotropic	110	950	1033

3.2.1 Elastic-plastic FE model of bi-material system

Figure 9a shows the C(T) specimen model by the plane strain element (8-node second order isoparametric element designated as CPE8 in ABAQUS; 15170 elements in total). A refined mesh is used at the crack tip and the quarter-node elements are used at the crack tip to capture the high stress gradient (Fig. 9b). The loading pin is simulated as a rigid body due to the relatively small deformation compared with the C(T) specimen. Interaction between the loading pin and C(T) specimen is simulated by the surface-to-surface contact pairs. Fig. 9 also shows the material property definition in the bi-material system. The isotropic hardening rule was used to specify the plastic behavior. The relationship between yield stress and plastic strain was defined in ABAQUS to model the stress-strain curve given in Ref [23]. Taking the type B as an example, the specimen is modelled by two material zones divided by the WAAM-substrate interface. The upper and lower zones are modelled by the WAAM and wrought Ti-6-4 properties, respectively.
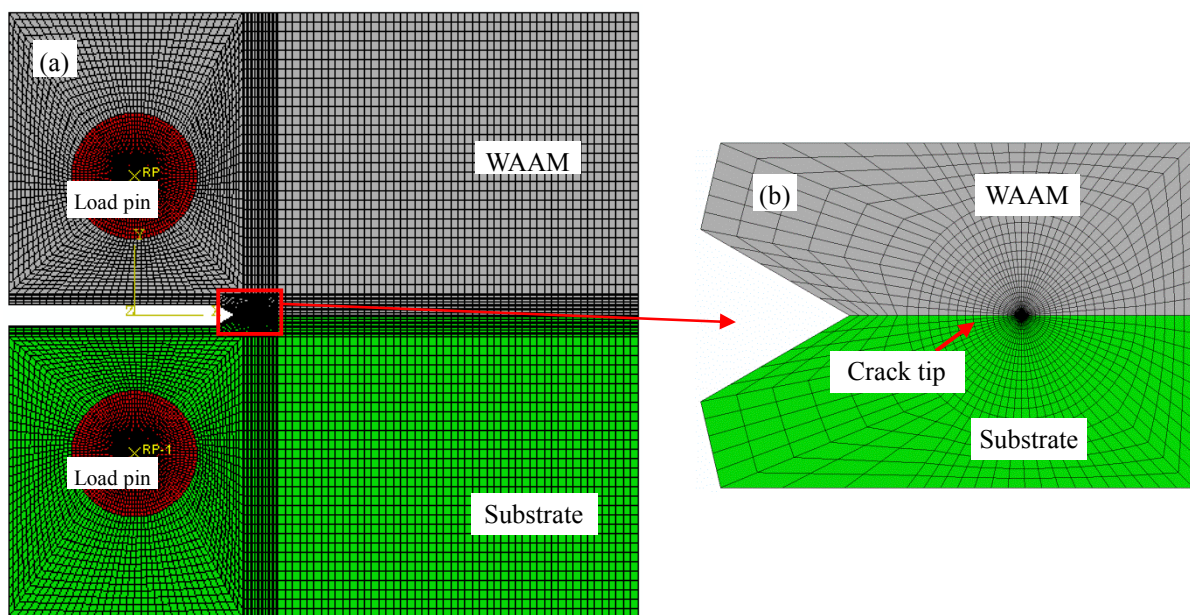

Fig. 9 Elastic-plastic finite element model of crack extension in bi-material system (Type B): (a) FE model of the C(T) specimen; (b) Detail mesh around the notch and crack tip area

3.2.2 Maximum tangential stress criterion in the elastic-plastic stress field

Since there is no criterion currently available in ABAQUS for predicting crack growth direction in an elastic-plastic material, in this paper, the Maximum Tangential Stress (elastic-plastic) criterion, named as the MTS$_P$ [41], was applied to estimate the crack trajectory at the WAAM-substrate interface. According to this criterion, the crack will propagate along the direction where the tangential stress is the greatest. Hence, the crack deviation angle (θ) can be determined by the following equation

$$\sigma_{T,max} = \max_{\theta}\left(\sigma_T(\theta)\right)_{R=r_{eval}} \tag{2}$$

where r_{eval} is the radial distance from the crack tip to the point where the crack deviation angle is evaluated, $\sigma_T(\theta)$ is the normal stress in the tangential direction that is obtained from the elastic-plastic FE model. Evaluation of crack deviation angle (θ) is performed by the following steps.

(1) Calculated stress components (σ_x, σ_y, τ_{xy}) are transformed from the global Cartesian coordinate (*x-y*) to the local cylindrical coordinate (*R-T*) system, as shown in the Figs. 10a and b.

(2) The tangential stress, $\sigma_T(\theta)$, at a given radius r_{eval} was recorded, where θ ranges from -180° to 180°, shown in Fig. 10c. At the evaluation point, distance to the crack tip r_{eval} must be smaller than the radius of the theoretical plastic zone [39], which is 0.104 mm by Irwin's plastic zone model [42] for Type B specimen. In this study, the tangential stress was evaluated at two points, i.e. r_{eval} equals 0.005 and 0.02 mm, as shown in Fig. 10c.
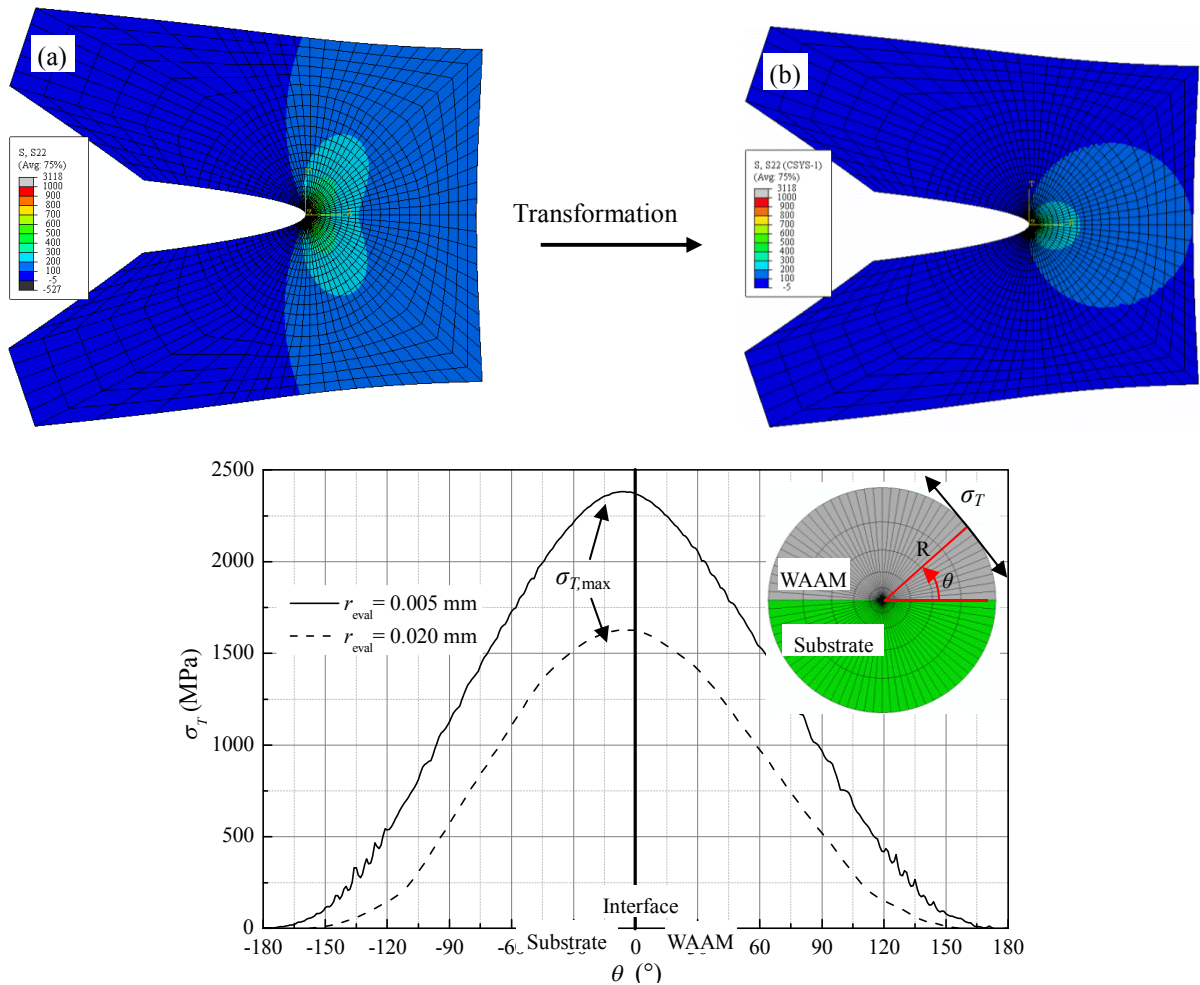

Fig.10 Calculated tangential stress distribution around the crack tip in (a) global coordinate (*x-y*) and (b) local cylindrical coordinate (*R-T*), (c) tangential stress $\sigma_T(\theta)$ at r_{eval}=0.005 and 0.02mm

(3) The angle where the tangential stress is the highest is the crack growth direction, according to the MTS_P criterion. It can be seen from Fig. 10c that the crack deviation angle is about -6.5° for the Type B specimen, i.e., crack tends to enter the substrate when it is initiated at the WAAM-Substrate interface.

4. Results and discussions

4.1 Crack path selection at the interface

Experimental test results in Section 2 have indicated that fatigue crack growth path around the interface is dependent on the initial crack orientation (i.e. either perpendicular or parallel to the interface). Crack maintains a straight path when it is perpendicular to the interface, whereas crack tends to grow into the wrought substrate when it is parallel to the interface. Influences of microstructure, residual stress and bi-material system on crack deviation tendency are analysed and discussed in the following sections.

4.2 Influence of microstructure and fatigue crack growth rate

Figure 11 shows the difference in the microstructure and crack growth rate [33] between the wrought and WAAM Ti-6-4. The fatigue crack growth rate of WAAM alloy in the T-L direction is also reported in Fig. 11c. Microstructure of the wrought alloy is the α+β equiaxed structure (Fig. 11a) that is the same as most high strength Ti-6-4 used in the airframes. The WAAM alloy has the Widmanstätten lamellar structure (Fig. 11b) that is also reported for WAAM [7] and other AM process deposited titanium alloys [10, 11].
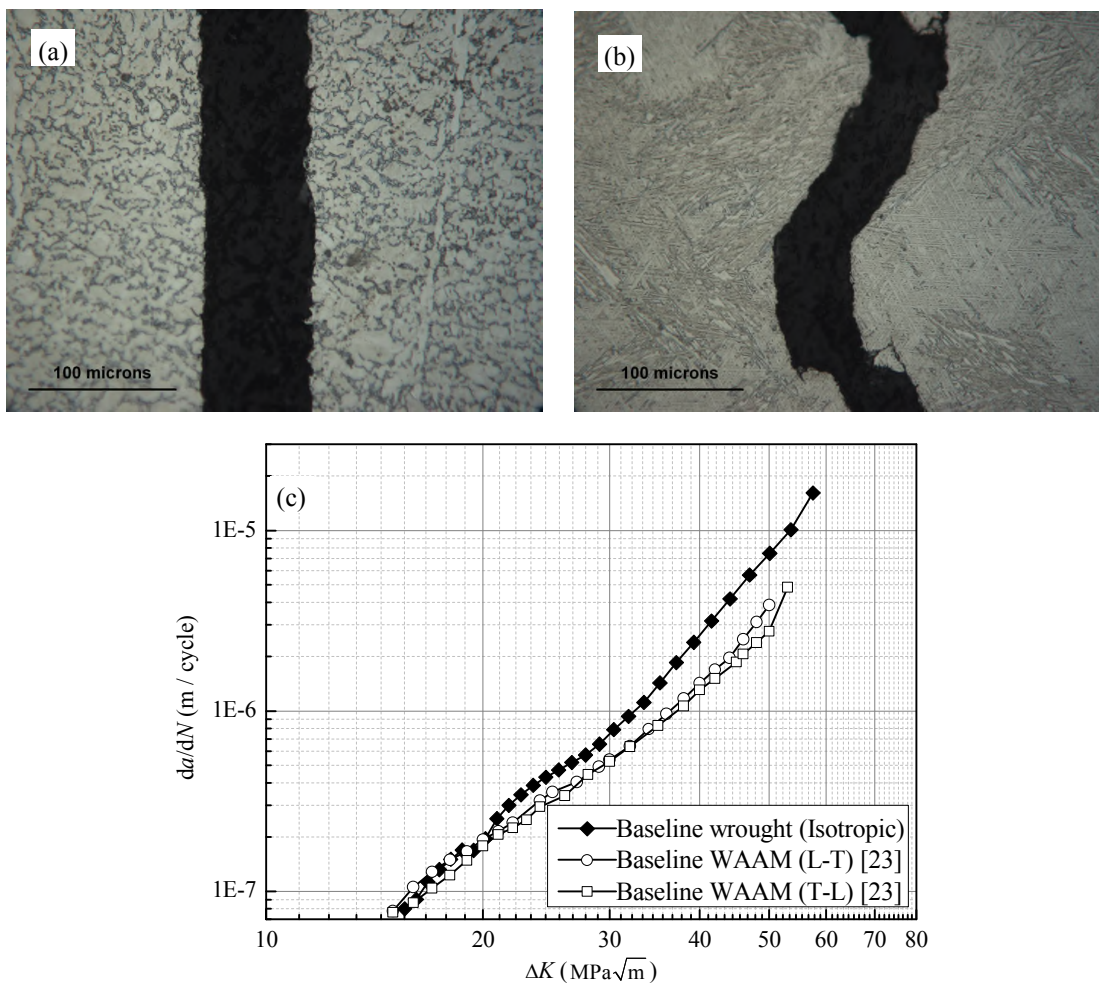

Fig. 11 Optical micrographs showing the crack growth pattern in the wrought substrate (a), WAAM (b), and comparison of fatigue crack growth rate da/dN vs. stress intensity factor range ΔK (c)

Differences in the microstructure can cause different resistance to fatigue crack propagation. In the substrate, cracks propagate smoothly in the fine α+β equiaxed structure and consequently have a higher growth rate (Fig. 11a and c). In the WAAM alloy, a crack takes a tortuous route owing to the lamellar structure which results in a slower growth rate (Fig. 11b and c). Fig. 11c shows that the WAAM Ti-6-4 exhibits a lower crack growth rate in both the longitudinal and transverse directions than that in the wrought alloy (isotropic) in the Paris law region (Region II). This is also reported by Edwards et al [14] for the electron beam melted Ti-6-4.

The relationship of the crack growth rate and stress intensity factor range characterizes the resistance to crack propagation under fatigue load. Comparisons shown in Fig. 11c indicate that WAAM Ti-6-4 has higher resistance to crack propagation than the wrought alloy used in the substrate. Cracks tend to propagate towards the material that has lower resistance to propagation when the crack is initiated at the WAAM-substrate interface and is parallel to the interface, i.e., cracks will grow into the substrate for the Type B, D and E specimens.

4.3 Influence of residual stress

FE models in Section 3.1 show that residual stress distribution is symmetric for the Type A and C specimens but asymmetric for the Type B, D and E. According to the maximum tangential stress criterion (eq. 1, elastic condition), the crack deviation angle induced by residual stress depends on the proportion of the applied maximum load to the residual stress. Table 4 provides the total stress intensity factor (K_{tot}) owing to the applied maximum load and residual stress, crack propagation angle (θ) that is estimated by eq. 1 based on the calculated $K_{I, tot}$ and $K_{II,tot}$.

As can be seen from Table 4, for the Type A and C specimens, the mode II stress intensity factor is zero ($K_{II,tot}= 0$) under the combined residual stress and applied load, hence the crack deviation angle is also zero, indicating that the crack keeps a straight propagation path in the Type A and C specimens (Figs. 3a and c). However, for the Type B, D and E specimens, residual stress results in considerable mode II stress intensity factor with positive values ($K_{II, tot} > 0$); consequently this results in negative crack deviation angle ($\theta < 0$), meaning that the cracks tend to propagate into the substrate alloy, as shown in Figs. 3 b, d and e. Furthermore, the prediction results show that Type E specimen has the maximum deviation angle, and Type D has the minimum angle value, which is in agreement with the experimental observations shown in Fig. 3.

Table 4 Calculated total stress intensity factor (K_{tot}) and the crack deviation angle (θ) under maximum applied load (P_{max}=5kN) and residual stress

| Type of Specimen	A	B	C	D	E
Crack length, a (mm)	30	17	30	17	17
K_I induced by applied maximum load, $K_{I, app}$ (MPa$\sqrt{m}$)	24.756	15.216	24.756	15.216	15.216
K_{II} induced by applied maximum load, $K_{II, app}$ (MPa$\sqrt{m}$)			0		
$K_{I,tot} = K_{I, app}+ K_{I, res}$ (MPa$\sqrt{m}$)	26.258	21.060	34.939	19.953	22.452
$K_{II,tot} = K_{II, app}+ K_{II, res}$ (MPa$\sqrt{m}$))	0.000	2.704	0.000	1.771	3.731
Crack deviation angle, θ (°)	0.000	-14.185	0.000	-9.990	-17.945

4.4 Influence of mechanical property mismatch

The mismatch of mechanical properties of WAAM and substrate Ti-6Al-4V is another factor which may cause the crack deviation at the interface. Crack path selection in the bi-material system of tested

samples was investigated using the elastic-plastic FE model described in Section 3.2. Calculated results are presented in two groups according to the crack growth direction with respect to the WAAM-Substrate interface.
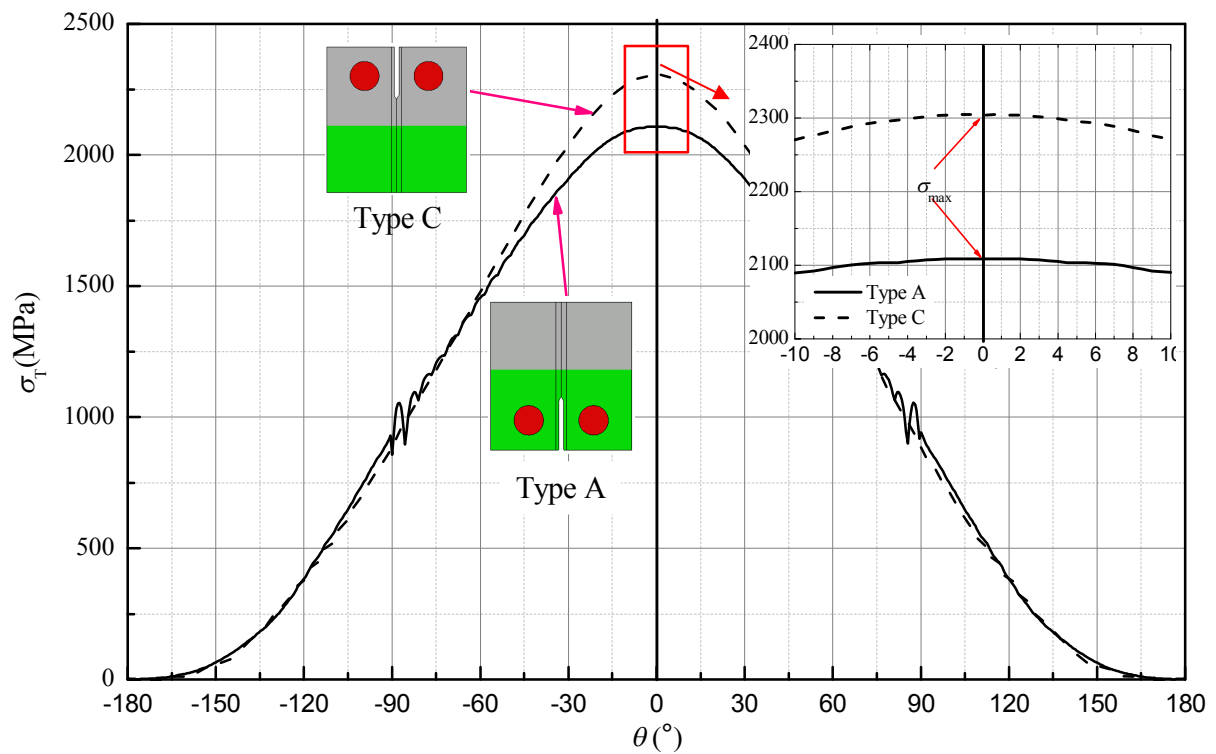
(a) Type A and C (a = 30 mm)
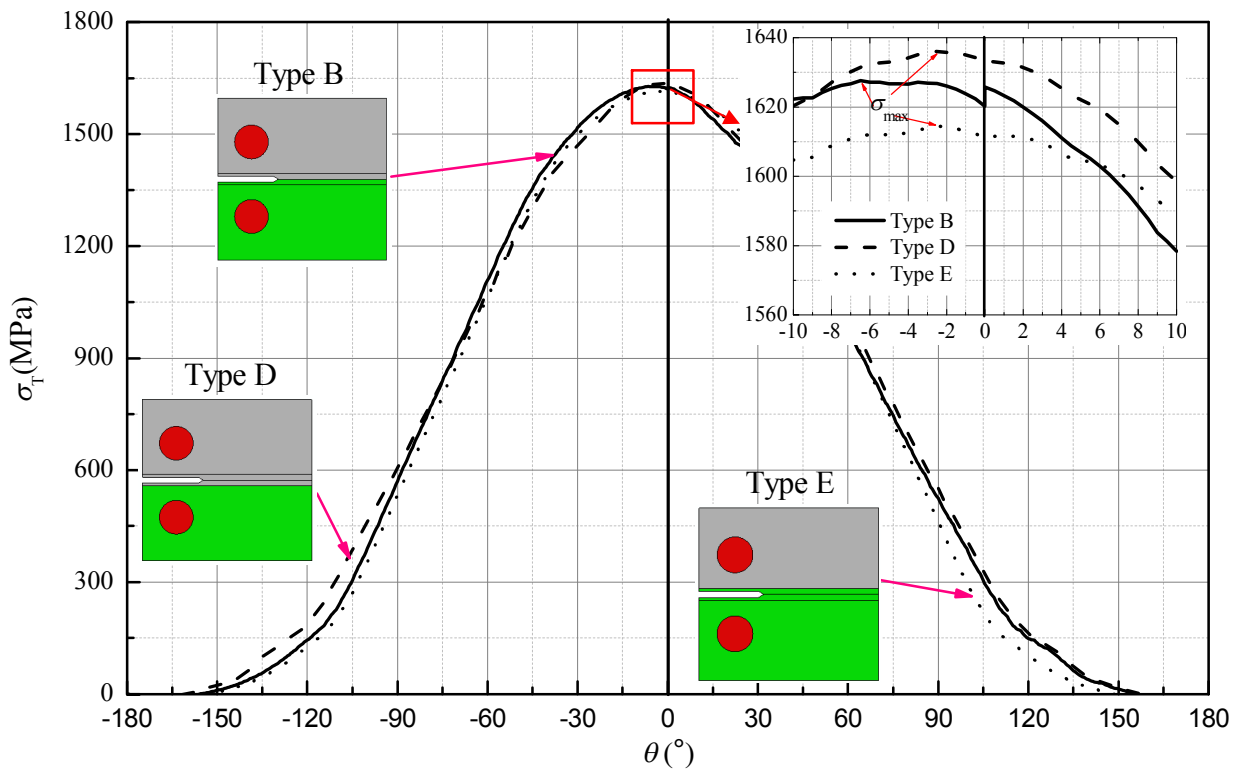
(b) Type B, D and E (a =17 mm)

Fig. 12 Calculated tangential stress around the crack tip (distance to tip r_{eval}=0.02mm)

15

For the Type A and C specimens (cracks propagate perpendicular to WAAM-Substrate interface), Fig. 12a shows the tangential stress distribution near the crack tip (r_{eval}= 0.02 mm) at the interface (a = 30 mm), i.e., the crack tip at the interface exactly. It should be noted that the crack tip plastic zone is located in the WAAM alloy zone for the Type A specimen but in the substrate zone for the Type C. Although Type A and C specimens give different tangential stress distribution due to the difference in mechanical properties, the tangential stress reaches its maximum value when $\theta = 0°$ for both specimens, indicating that cracks will follow a straight growth path when propagating perpendicular to WAAM-Substrate interface.

For the Type B, D and E specimens (cracks grow parallel to the interface), Fig. 12b shows the tangential stress distribution around the crack tip (r_{eval}= 0.02 mm) when a=17 mm, i.e. at the beginning of the fatigue crack growth test. Unlike the case of symmetric residual stress distribution for Type A and C specimens, an asymmetric stress distribution is caused by the mismatch in mechanical properties between the WAAM and substrate alloys. The tangential stress reached its maximum value at θ = -6.5, -2 and -2° for Type B, D and E, respectively. According to the MTS_P criterion presented in Section 3.2, cracks will tend to deviate into the substrate.

It should be pointed that this paper aims to explain the crack propagation tendency at the WAAM-Substrate surface. Although the FE models (containing residual stress and bi-material properties) provide the same deviation tendency as the experimental results, the calculated deviation angle only represents the tendency of initial deviation. Since the deviation angle is a function of stress intensity factors ($K_{I,tot}$ and $K_{II,tot}$), it is strongly related to the growing crack length. Crack deviation continues during the subsequent crack propagation process, therefore as the crack gets longer, it will in turn impact the residual stress redistribution and the stress intensity factor values; hence the deviation angle. A more complex model needs to be developed to predict the continuing change in the crack deviation angle and crack growth path, which is beyond the scope of this paper and will be the subject of future work.

5. Conclusions

Crack propagation deviation tendency in specimens containing an interface between wrought substrate and WAAM Ti-6Al-4V is investigated from the microstructure, residual stress and bi-material points of view. FEA has been performed to explain the effects of residual stress and bi-material properties. The following conclusions can be drawn.

(1) Since the lamellar structured WAAM alloy has lower crack growth rate than that in the equiaxed wrought condition, cracks have a tendency to grow towards the wrought substrate when they are initiated at and in parallel with the WAAM-substrate interface.

(2) Residual stress distribution is symmetric in the Type A and C but asymmetric for the Type B, D and E specimens. Cracks keep a straight propagation path in the Type A and C specimens, since the mode II stress intensity factors induced by residual stress are zero. For the Type B, D and E specimens, residual stress results in a considerable mode II stress intensity factor that leads to crack path deviation into the substrate.

(3) The mismatch of the material elastic and plastic mechanical properties between the WAAM and wrought alloys also has an influence on the crack path selection. The bi-material FE model shows that when cracks propagate perpendicular to the WAAM-substrate interface, the tangential stress is symmetric and reached a maximum value at θ = 0. Asymmetric tangential stress is found when cracks grow parallel to WAAM-substrate interface. According to the maximum tangential stress criterion,

crack will deviate into the substrate.

In summary, all three influential factors (microstructure, residual stress and bi-material properties) support the experimentally observed crack deviation trend, i.e., crack deviates into the substrate when it initiates at and in parallel with the WAAM-substrate interface.

Acknowledgement

References

[1] M. Peters, J. Kumpfert, C.H. Ward, et al, Titanium alloys for aerospace applications. Adv Eng Mater 5(2003) 419-27

[2] F. Martina, J. Mehnen, S.W. Williams, et al, Investigation of the benefits of plasma deposition for the additive layer manufacture of Ti-6Al-4V, J. Mater. Process. Technol. 212 (2012) 1377-1386

[3] F. Wang, S.W. Williams, M. Rush. Morphology investigation on direct current pulsed gas tungsten arc welded additive layer manufactured Ti6Al4V alloy, Int. J. Adv. Manuf. Tech. 57 (2011) 597-603

[4] E. Brandl, B. Baufeld, C Leyens, et al, Additive manufactured Ti-6AL-4V using welding wire: comparison of laser and arc beam deposition and evaluation with respect to aerospace material specifications, Phys. Procedia. 5 (2010) 595-606

[5] W.E. Frazier, Metal Additive Manufacturing: A Review, J. Mater. Eng. Perform. 23 (2014) 1917- 1928

[6] B. Baufeld, E. Brandl, O Van der Biest, Wire based additive layer manufacturing: comparison of microstructure and mechanical properties of Ti-6Al-4V components fabricated by laser-beam deposition and shaped metal deposition. J. Mater. Process. Technol. 211 (2011) 1146-1158

[7] F. Wang, S.W. Williams, P. Colegrove, et al, Microstructure and mechanical properties of wire and arc additive manufactured Ti-6Al-4V, Metall. Mater. Trans. A 44 (2013) 968-977

[8] B. Baufeld, O. Van der Biest, R. Gault, Additive manufacturing of Ti-6Al-4V components by shaped metal deposition: microstructure and mechanical properties, Mater. Des. 31 (2010) S106- S111

[9] E. Brandl, F. Palm, V. Michailov, et al, Mechanical properties of additive manufactured titanium (Ti-6Al-4V) blocks deposited by a solid-state laser and wire, Mater. Des. 32 (2011) 4665- 4675.

[10] S.H. Mok, G. Bi, J Folkes, et al, Deposition of Ti-6Al-4V using a high power diode laser and wire, Part II: Investigation on the mechanical properties, Surf. Coat. Tech. 202 (2008) 4613-4619.

[11] S. Leuders, M. Thöne, A. Riemer, et al, On the mechanical behaviour of titanium alloy TiAl6V4 manufactured by selective laser melting: Fatigue resistance and crack growth performance. Int. J. Fatigue, 48 (2013) 300-307

[12] P. Edwards, M. Ramulu, Fatigue performance evaluation of selective laser melted Ti–6Al–4V, Mater. Sci. Eng., A 598 (2014) 327-337.

[13] B. Van Hooreweder, D. Moens, R. Boonen, et al. Analysis of fracture toughness and crack propagation of Ti6Al4V produced by selective laser melting, Adv. Eng. Mater., 14(2012) 92-97.

[14] P. Edwards, M. Ramulu, Effect of build direction on the fracture toughness and fatigue crack growth in selective laser melted Ti-6Al-4V, Fatigue Fract. Engng. Mater. Struct., 38 (2015) 1228- 1236.

[15] P. Edwards, A. O'Conner, M. Ramulu, Electron beam additive manufacturing of titanium components: properties & performance, J. Manuf. Sci. E-T ASME, 135 (2013): 061016/1-7

[16] P.A. Colegrove, H.E. Coules, J. Fairman, et al. Microstructure and residual stress improvement in wire and arc additively manufactured parts through high-pressure rolling. J. Mater. Process. Technol. 213 (2013) 1782-1791

[17] Y. Zhu, D. Liu, X. Tian, et al, Characterization of microstructure and mechanical properties of laser melting deposited Ti–6.5Al–3.5Mo–1.5Zr–0.3Si titanium alloy. Mater. Des. 56 (2014): 445-53

[18] S.M. Kelly, S.L. Kampe, Microstructural evolution in laser-deposited multilayer Ti-6Al-4V builds: part I. microstructural characterization, Metall. Mater. Trans. A 35 (2004) 1861-1867

[19] K. Taminger, R. Hafley, Electron beam freeform fabrication for cost effective near-net shape manufacturing. NATO/RTOAVT-139 Specialists' Meeting on Cost Effective Manufacture via Net Shape Processing, Amsterdam, the Netherlands, 2006: 9-25

[20] A.A. Antonysamy, J. Meyer, P.B. Prangnell, Effect of build geometry on the β-grain structure and texture in additive manufacture of Ti-6Al-4V by selective electron beam melting. Mater. Charact. 84 (2013) 153-168

[21] G. Schroeder, J. Albrecht, G. Luetjering. Fatigue crack propagation in titanium alloys with lamellar and bi-lamellar microstructures. Mater. Sci. Eng., A 319-321 (2001) 602-606.

[22] A.A. Antonysamy, Microstructure, texture and mechanical property evolution during additive manufacturing of Ti6Al4V alloy for aerospace applications, PhD Thesis, 2012, University of Manchester

[23] E. Lorant, Effect of microstructure on mechanical properties of Ti-6Al-4V structures made by additive layer manufacturing. MSc Thesis, 2010, Cranfield University

[24] A.G. Evans, B.J. Dalgleish, M. He, et al. On crack path selection and the interface fracture energy in bimaterial systems. Acta Mater. 37 (1989) 3249–3254

[25] P. Nègre, D. Steglich, W. Brocks. Crack extension at an interface: prediction of fracture toughness and simulation of crack path deviation. Int. J. Fracture. 134(2005) 209-229.

[26] K. Fan, G.Z. Wang, F.Z. Xuan, et al. Effects of work hardening mismatch on fracture resistance behavior of bi-material interface regions. Mater. Des. 68(2015) 186–194

[27] J. Ding, P. Colegrove, J. Mehnen, et al, Thermo-mechanical analysis of wire and arc additive layer manufacturing process on large multi-layer parts. Comput. Mater. Sci. 50 (2011) 3315-3322

[28] P. Rangaswamy, T.M. Holden, R.B. Rogge, et al. Residual stresses in components formed by the laser-engineered net shaping (LENS®) process, J. Strain Anal. Eng. Des. 38 (2003) 519-527

[29] A. Paradowska, J.W.H. Price, R. Ibrahim, et al, A neutron diffraction study of residual stress due to welding, J. Mater. Process. Technol. 164-165 (2005): 1099-1105

[30] N. Hills, Fatigue crack propagation behaviour at the interface of additively manufactured Ti-6Al-4V and the substrate. MSc Thesis, 2014, Cranfield University

[31] Zhang X. Fatigue & fracture behaviour of additively manufactured Ti-6Al-4V, Presented at WAAMMat Industrial Day, Bedford, UK, March 31, 2015 (unpublished).

[32] A. Addison, J. Ding, F. Martina, et al, Manufacture of complex titanium parts using Wire+Arc Additive Manufacture, Titanium Europe 2015 - International Titanium Association, 11-13 May 2015, Birmingham, UK

[33] J. Zhang, X. Wang, S. Paddea, X. Zhang, Fatigue crack propagation behavior in wire+arc additive manufactured Ti-6Al-4V: effects of microstructure and residual stress. Mater. Des. 90 (2016): 551-561

[34] ASTM E647-13. Standard Method for measurement of fatigue crack growth rates, American Society for the Testing of Materials, 2013

[35] M.B. Prime. Cross-sectional mapping of residual stresses by measuring the surface contour after a cut[J]. J Eng Mater-T ASME, 123, 2001:162-168

[36] M. B. Prime, R. J. Sebring, J. M. Edwards, et al. Laser surface-contouring and spline data-smoothing for

residual stress measurement. Exp. Mech., 44(2004) 176–184

[37] V. Dattoma, M. De Giorgi, R. Nobile, On the evolution of welding residual stress after milling and cutting machining. Comput. Struct. 84 (2006) 1965-1976

[38] Abaqus 6.13. Abaqus Analysis User's Manual 11.2.1: Element and contact pair removal and reactivation.

[39] Abaqus 6.13. Abaqus Theory Manual 2.16.4: Prediction of the direction of crack propagation

[40] R. Pippan, F.O. Riemeloser, Fatigue of bimaterials. Investigation of the plastic mismatch in case of cracks perpendicular to the interface. Comp. Mater. Sci. 13(1998) 108-116.

[41] P. Dahlin, M. Olsson, The effect of plasticity on the incipient mixed-mode fatigue crack growth. Fatigue Fract. Eng. M. 26(2003) 577-588

[42] G.R. Irwin, Linear fracture mechanics, fracture transition, and fracture control. Eng. Fract. Mech., 1968,1:241–257

2016-05-12

Crack path selection at the interface of wrought and wire + arc additive manufactured Ti–6Al–4V

Zhang, Jikui